Theoretical and Applied Fracture Mechanics 54 (2010) 44–53

Contents lists available at ScienceDirect

Theoretical and Applied Fracture Mechanics

journal homepage: www.elsevier.com/locate/tafmec

Dynamic crushing characteristics of high strength steel cylinders with elliptical geometric discontinuities

M.Y. Huang [a], Y.S. Tai [b,*], H.T. Hu [a]

[a] Department of Civil Engineering, National Cheng Kung University, Taiwan, ROC
[b] Department of Civil Engineering, ROC Military Academy, Taiwan, ROC

ARTICLE INFO

Article history:
Available online 19 June 2010

Keywords:
High-strength steel
Impact
Axial compression
Thin-walled cylinders
Cutout

ABSTRACT

Thin-walled members are commonly used as energy absorbers in engineering structures and often contain cutouts. This study performed numerical simulations of high strength steel cylindrical shells with elliptical cutouts subjected to dynamic axial impact. The LS-DYNA code was the primary analytical tool used to analyze the influence of cutout locations, cutout shapes and symmetry of cutout on the energy absorption capabilities and the crush characteristics of tubes with a cutout. For high strength steel tubes made from a rate sensitive material, the stress–strain curves of different strain rates were used to elucidate the effect of dynamic impact on the strain rate. Our results show that collapse crushing behavior is strongly influenced by the location and symmetry of cutouts and the variation of major axis influences the peak crush load.

1. Introduction

Thin-walled circular cylindrical shells are an excellent mechanism for energy absorption and have been widely used in engineering structures such as automobiles, aircraft, military facilities, bridge structures and other applications because of high load carrying capacity and low structural weight. These components in service are commonly subjected to axial compressive loading. It is well known that, the energy absorbing ability of structures depends on various crushing failure mode. The deformation mode and energy absorption efficiency of thin-walled tubes are strongly correlated with each other. Previous studies developed models for analyzing the axial bucking property of thin-walled members based on plastic hinge theory, experimentation or numerical simulation [1–8]. In the past investigations of cylindrical shell under various kinds of external loading conditions, the work in [1] have observed axi-symmetrical fold pattern of a circular tube under quasi-static loading during an experiment. He proposed the concept of the static plastic hinge theoretical model and deduced a simple expression for the mean crushing force. For improving this solution, conducted in [2] considered both axi-symmetrical and non-symmetrical modes and developed concepts regarding crushing forces, respectively. They also carried out experiments on circular and square steel tubes and compared the results with theoretical predictions. Adopted in [3] is the LS-DYNA to perform a numerical simulation investigates the behavior of hat-shaped cross-sections of various materials under axial crushing. Analyzed is also the effect of the hat-height and initial imperfections on collapse behavior and compared their results with experimental data.

Factors that influence the deformation mode and the crushing of high strength steel extrusions include material properties, structure geometry, discontinuities and loading conditions. Though previous research on the crushing behavior of thin-walled tubes made of materials with and without strain hardening and strain rate effects has been reported, studies utilizing tubes containing a cutout are limited. In addition, these shell structures often contain complex stiffeners and cutouts, as a result of practical needs; these geometric discontinuities can cause a stress concentration response near the cutout and subsequently influence the deformation mode of the structure. As a result, the discontinuous problem of thin-walled tubes has attracted the attention of several researchers in recent years. Many studies have been conducted which show that a cutout in a shell structure can have a significant effect on the response of the shell [9–12]. Conducted in [9] found that by introducing crush initiators into structural members, a splitting and cutting deformation mode was generated rather than a globing bending deformation which has been observed for specimens without any discontinuities. Presented in [10] was to compare the crush characteristics and energy absorption capacity of three different types and major axis lengths of geometrical discontinuities located at mid-height using numerical simulation modeling. The response of aluminum and steel tubes containing a square cutout subject to both quasi-static and dynamic impact loadings have been previously investigated. From that study, an understanding of the effects of material properties, strain rate effect, location of cutouts, tube

* Corresponding author.
E-mail address: ystai@cc.cma.edu.tw (Y.S. Tai).

0167-8442/$ - see front matter © 2010 Elsevier Ltd. All rights reserved.
doi:10.1016/j.tafmec.2010.06.014

length and impact speed on the crushing behavior and energy absorption capacity was gained.

Due to the higher strength and excellent formability, high-strength steel is gradually becoming more popular in replacing conventional steel materials in recent years. Energy absorption capabilities are important in improving the crashworthiness without increasing structural weight. Previous results have indicated that a cutout in a shell structure causes a local response to occur near the cutout when the shell is subjected to load. More information is needed regarding the crushing behavior of high-strength steel sections with cutouts. This study used the nonlinear finite element code LS-DYNA to establish an efficient and economic analysis model for predicting the energy absorption characteristics and dynamic crushing collapse mode of the discontinuous structures. In addition, the crush characteristics of high strength steel cylinders with different elliptical shape discontinuities is investigation to understand the optimal configuration of a cutout in a thin-walled shell. Results of this study provide a valuable reference for future applications and design.

2. Theoretical background [13]

2.1. Governing equations

When tube is subjected to an impact load, the governing equations are:

Equation of mass conservation:

$$\rho V = \rho_0 \tag{1}$$

where V represents the relative volume; ρ denotes the current density, and ρ_0 denotes the reference density.

Equation of momentum conservation:

$$\sigma_{ij,j} + \rho f_i = \rho \ddot{u}_i \tag{2}$$

where σ_{ij} represents the Cauchy stress; f_i represents the body force density, and $\ddot{u}_i$ denotes the acceleration.

Equation of energy conservation:

$$\dot{E} = V s_{ij} \dot{\varepsilon}_{ij} - (p+q)\dot{V} \tag{3}$$

where s_{ij} and p denote the deviatoric stresses and hydrostatic pressure, respectively, as given in

$$s_{ij} = \sigma_{ij} + (p+q)\delta_{ij} \tag{4}$$

where q represents the bulk viscosity; δ_{ij} denotes the Kronecker delta ($\delta_{ij} = 1$, if $i = j$; otherwise $\delta_{ij} = 0$), and $\dot{\varepsilon}_{ij}$ denotes the strain rate tensor.

$$p = -\frac{1}{3}\sigma_{ij}\delta_{ij} - q = -\frac{1}{3}\sigma_{kk} - q \tag{5}$$

Based on the virtual work principle, Eq. (2) can be expressed as a weak form of equilibrium equation

$$\int_v (\rho \ddot{u}_i - \sigma_{ij,j} - \rho f)\delta u_i dv + \int (\sigma_{ij} n_j - t_i)\delta u_i ds + \int \left(\sigma_{ij}^+ - \sigma_{ij}^-\right) n_j \delta u_i ds = 0 \tag{6}$$

where δu_i fulfills all boundary conditions, and the integrations are over the current geometry. Application of the divergence theorem gives

$$\int_v (\sigma_{ij}\delta u_i)_{,j} dv = \int \sigma_{ij} n_j \delta u_i ds + \int \left(\sigma_{ij}^+ - \sigma_{ij}^-\right) n_j \delta u_i ds \tag{7}$$

and noting that

$$(\sigma_{ij}\delta u_i)_{,j} \sigma_{ij,j}\delta u_i = \sigma_{ij}\delta u_{i,j} \tag{8}$$

leads to the weak form of the equilibrium equations:

$$\delta\pi = \int_v \rho \ddot{u}_i \delta u_i dv + \int_v \sigma_{ij}\delta u_{i,j} dv - \int_v \rho f_i \delta u_i dv - \int t_i \delta u_i ds = 0 \tag{9}$$

If the finite element technique is interconnected using a matrix form, Eq. (9) becomes

$$\sum_{m=1}^{n} \left\{ \int_{v_m} \rho N^t N a dv + \int_{v_m} B^t \sigma d v - \int_{v_m} \rho N^t b dv - \int_{\partial b_1} N^t t ds \right\}^m = 0 \tag{10}$$

where N is an interpolation matrix, σ is the stress vector, B is the strain-displacement matrix, a is the nodal acceleration vector, b is the body force load vector, and t are applied traction loads. The equation is integrated in time and is applied to evaluate the equation of state and for a global energy balance

2.2. Adaptive meshing

A rigid mass impact causes severe deformation of the target cylinders. As a result of which the elements in top of the cylinders get heavily distorted, leading to the negative element volume and consequent error termination of the program. To defeat the problem of excessive element distortion h-adaptive meshing of LS-DYNA was used in all cases of cylinders impacted by rigid mass. The method's elements are subdivided into smaller elements wherever an error indicator shows that subdivision of the elements will provide improved accuracy. During an h-adaptive process, parts of the mesh are selectively refined using linear interpolation during the course of the solution procedure; this process is called fission [13]. Refinement indicators are used to decide the locations of mesh refinement. One deformation based approach checks for a change in angles between adjacent elements. The adaptive process is consisting of several levels of fission. When one element is divided into four elements, this step is referred to as the second refinement. In subsequent steps, the fissioned elements can again be fissioned in a third refinement, and these elements can again, in turn, be fissioned in to a fourth (see Fig. 1). The frequency of adaptive meshing affects the mesh quality. A typical problem of high rate of deformation requires a more frequent adaptive meshing. In the present problem adaptive meshing was performed at every five increments of the analysis.

3. Numerical simulations

3.1. Description of numerical model

The general geometry and FEM model of the shells analyzed in this study is defined in Fig 2. The dimensions of the extruded tube for all of the model configurations were $L = 200$ mm, $D = 58$ mm, $t = 1.4$ mm and the variation of L_0 was considered. The distance between the centers of the cutout to the bottom end of the tube is denoted as L_0. The tests were conducted at velocity 12.14 m/s with an

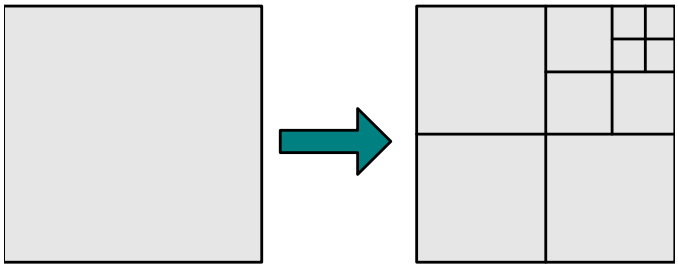

Fig. 1. Quadrilateral element fissioned to the fourth level [13].

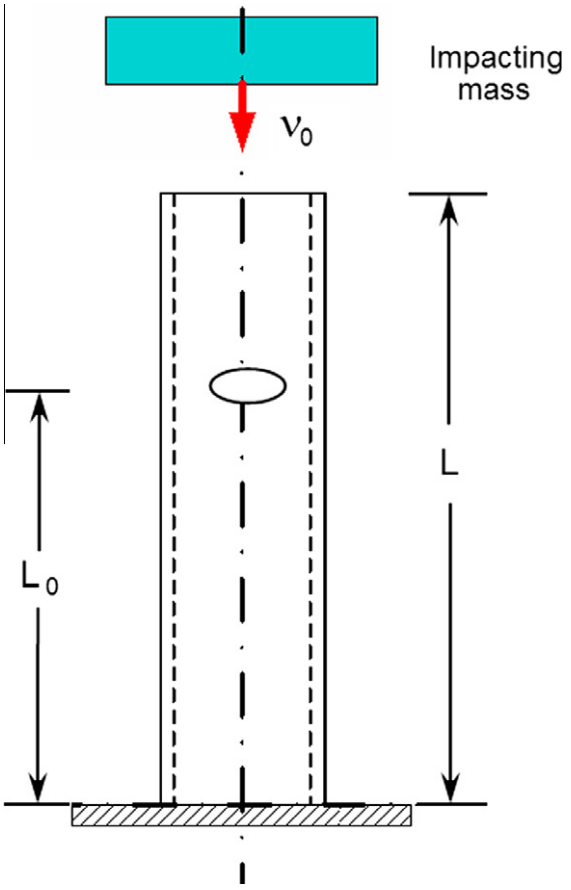

Fig. 2. Geometries and FEM model of the cylindrical shell and discontinuities under consideration.

impacting mass of 117 kg to assess crushing behavior. Elliptical holes with different major axis lengths and aspect ratios were selected as the geometrical discontinuities. All circular tubes with various cutouts and different locations of holes along the lengths were numbered, as presented in Tables 1 and 2.

The thin-walled sections in this study were made of high strength steel, a strain rate sensitive material having Young's modulus E = 195 GPa, density = 7850 kg/m^3 and the value of yield stress σ_0 = 495 MPa. In order to gain accurate numerical results, the stress–strain curves of different strain rates used in the numerical simulation are presented in Fig. 3 that were obtained from tensile tests using Hopkinson Split Bar.

Simulation using a whole model was used for analysis because of uncertainty in the destruction pattern. According to pass investigation [14,15], to display fully the buckling pattern of the structure and to make the outcome of the simulation more consistent with actual overlapping compression, the mesh must be smaller than half of the stress wavelength or the length of the plastic hinge.

Because the minimum thicknesses of the thin-walled components in this investigation were 1.4 mm, an optimal mesh size of 2.0 mm was used to model the cylindrical shells with and without cutout. Furthermore, in order to model the deformation behavior of the tubes more perfectly and consistent with the actual situation, a mesh study was conducted by using the ADAPTIVE command of LS-DYNA as described in Section 2.2.

All the tubes were modeled using Belytschko–Tsay four-node shell elements with five integration points through the thickness and one integration point in the element plane. The element type has a lumped mass matrix as required by the explicit calculation scheme and is suitable for the large deformations. The meshed shell elements were located at the mid-surface of the tube's wall and the stiffness-type hourglass control model was adopted to eliminate the zero-energy modes. The stress–strain curves describe strain rate effects of the material and were employed accordingly in the LS-DYNA simulations using the Type 24 MAT_PIECEWISE_LINEAR_PLASTICITY constitutive law of material card. The primary advantage of this material lies in the fact that it can simultaneously completely display characteristics of the plastic phase and an elasto-plastic material with any arbitrary stress versus strain curve and arbitrary strain rate dependency can be defined.

For simulation of the dynamic axial crushing, the bottom end of the tube was assumed to be built-in and was constrained in all degrees of freedom. The upper end was set free and subject to compression by the rigid loading plate with certain downward initial velocity of V_0. The loading plate is modeled as a rigid wall with a mass of m_0. In order to prevent penetration and sliding between

Table 1
Specimen detail and numerical simulation of circular tubes with one or two cutout placed in different locations.

No	Geometric description					Analytic results					
	Shape	L_0 (L)	Major axis (mm)	Minor axis (mm)	Aspect ratio	P_{max} (kN)	$P_{m\ (peak)}$ (kN)	P_m (kN)	$E_{absorbed}$ (kJ)	Deformation (mm)	Deformation mode[b]
C0			NO	NO	NO	173.78	146.41	77.64	8.57	114.51	MP
C10		0.50	4.0	14.05	0.285	162.41	138.51	35.99	3.511	120[a]	GB
C11		0.625				158.00	137.39	67.25	8.074	120[a]	GB
C12		0.75				157.16	137.44	78.88	8.526	107.17	PD
C13		0.875				158.42	137.69	75.02	8.522	113.44	PD
C14		0.50				153.36	127.12	61.61	7.273	133.3	PD
C40		0.50	7.62	7.62	1	159.42	134.78	40.94	3.694	120[a]	GB
C41		0.625				155.71	133.58	52.60	6.114	120[a]	GB
C42		0.75				155.76	133.9	74.03	8.484	112.41	PD
C43		0.875				155.35	134.76	73.29	8.538	116.98	PD
C44		0.50				149.96	120.39	71.05	8.542	116.81	PD
C90		0.50	16.0	3.62	4.422	144.68	122.00	34.97	3.613	120[a]	GB
C91		0.625				141.47	120.38	31.21	3.443	120[a]	GB
C92		0.75				141.49	120.76	70.31	8.495	120.2	PD
C93		0.875				139.28	122.02	73.62	8.514	117.09	PD
C94		0.50				121.75	95.90	66.99	8.381	117.8	PD

[a] Resulting in global bending and to clarify the results in comparison, the deformation of 120 mm was only considered.
[b] MP-mixed progressive folding, GB-global bending, PD-irregular progressive folding and initial folding occurred at around the geometrical discontinuity.

Table 2
Specimen detail and impact test results for different cutout tubes.

No	Geometric description					Analytic results					
	Shape	L_0 (L)	Major axis (mm)	Minor axis (mm)	Aspect ratio	P_{max} (kN)	$P_{m\ (peak)}$ (kN)	P_m (kN)	$E_{absorbed}$ (kJ)	Deformation (mm)	Deformation mode[a]
C12		0.75	4.0	14.05	0.285	157.16	137.18	78.88	8.526	107.17	PD
C22		0.75	5.0	11.37	0.440	157.22	136.37	74.66	8.534	114.67	PD
C32		0.75	7.0	8.20	0.854	156.27	134.63	73.99	8.534	113.72	PD
C42		0.75	7.62	7.62	1	155.76	133.90	74.03	8.484	112.41	PD
C52		0.75	9.0	6.40	1.405	154.29	132.24	73.39	8.538	115.02	PD
C62		0.75	11.0	5.25	2.095	151.57	129.57	73.14	8.526	115.77	PD
C72		0.75	13.0	4.45	2.922	148.43	126.32	73.35	8.523	115.75	PD
C82		0.75	14.0	4.13	3.387	145.43	123.88	72.57	8.495	117.15	PD
C92		0.75	16	3.618	4.422	141.49	120.76	70.31	8.495	120.20	PD

[a] PD-irregular progressive folding and initial folding occurred at around the geometrical discontinuity.

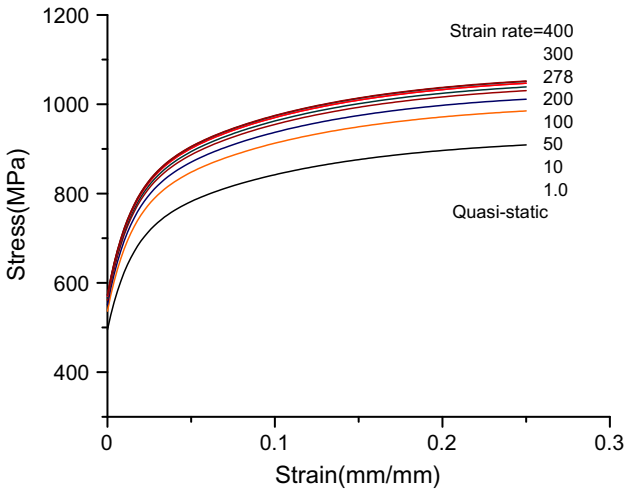

Fig. 3. Stress–plastic strain curves at different strain rates.

the rigid loading plate and the upper end of the tube during contact, the interface used the CONTACT_CONSTRAINT_NODES_TO SURFACE command of LS-DYNA and the friction coefficient between the contact surfaces were set to 1.0. Furthermore, when the thin-walled tube experiences overlapping shrinkage, the contact property between the lobes used a self-contact algorithm, CONTACT-AUTOMATIC-SINGLE-SURFACE with a friction coefficient of 0.1, preventing the lobes from penetrating each other during the deformation process.

3.2. Surface area of an elliptic cutout on a cylindrical shell

For practical considerations, a cylindrical shell was intersected with a small pipe whose cross section is an ellipse with radii a and b due to connective needs. Therefore, a cylindrical shell with an elliptic cutout was used (Fig. 4). The geometry of the elliptic pipe can be described by the equation

$$y = b\sqrt{1-\frac{z^2}{a^2}} \tag{11}$$

This must be satisfied on the boundary of the cutout. Now let us slice off a small strip (shadow area in Fig. 4) from the curved cutout surface. The area of this strip can be written as:

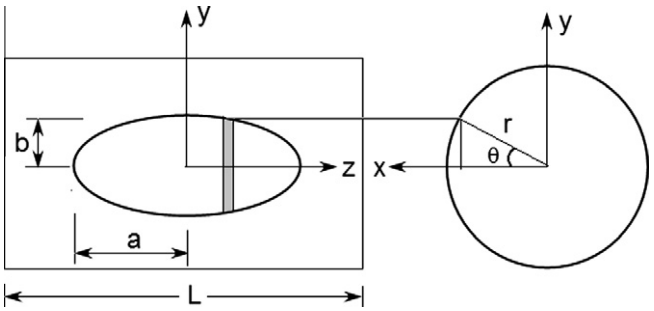

Fig. 4. Geometry of the elliptic cutout on a cylindrical shell.

$$dA = 2r\theta\, dz \tag{12}$$

From Fig. 4, the relation between θ and y is as follows

$$\sin\theta = \frac{y}{r} \tag{13}$$

Substituting Eq. (11) into Eq. (13) and solving for θ, we obtain

$$\theta = \sin^{-1}\left[\frac{b}{r}\sqrt{1-\frac{z^2}{a^2}}\right] \tag{14}$$

Substituting Eq. (14) into Eq. (12), we get

$$dA = 2r\sin^{-1}\left[\frac{b}{r}\sqrt{1-\frac{z^2}{a^2}}\right]dz \tag{15}$$

The total area of the cutout surface, A^*, then can be calculated by integrating Eq. (15). It has the following form:

$$A^* = \int_{-a}^{a} 2r\sin^{-1}\left[\frac{b}{r}\sqrt{1-\frac{z^2}{a^2}}\right]dz \tag{16}$$

or

$$A^* = 4r\int_{0}^{a} \sin^{-1}\left[\frac{b}{r}\sqrt{1-\frac{z^2}{a^2}}\right]dz \tag{17}$$

This constraint condition can be rewritten as $A^* = A/\alpha$, or

$$4r\int_{0}^{a} \sin^{-1}\left[\frac{b}{r}\sqrt{1-\frac{z^2}{a^2}}\right]dz = 2\pi rL/\alpha \tag{18}$$

In this study, α was selected as 200 for illustrative purposes. This constraint reduces the number of independent geometric parameters from two to one. The constraint equation can be solved numerically. The explicit relationship between radii a and b for a typical shell with an elliptic cutout is shown in Fig. 5

4. Results and discussion

Numerical simulations of crushing behavior were carried out for thin-walled tubes with a cutout of the same size located at different location, the variation of major axis length and symmetry of cutout subject to dynamic axial impact loading. The modeling results, shown in Tables 1 and 2 and Figs. 6–14, illustrate the overall behavior of thin-walled shells with geometrical discontinuities and the effects of cutouts on the response of energy absorbing capacity.

It could observed from the variations in principle collapse modes are either global bending or irregular folding caused of the geometrical discontinuities. For greater clarity, the mean value of the crushing force is the primary parameter used for comparisons. The energy absorption, E_a, of each specimen can be determined by integrating the force–deformation curve. Furthermore, the mean crushing force (P_m) calculated by dividing E_a by the axial crushing deformation. Due to the effects of geometrical discontinuities, fluctuations occurred in the axial mean crushing force following the peak force. The mean crushing force in this study was defined as an average of P_m in different deformations (see Fig. 6).

4.1. The effect of the location of the cutout

A cutout size of 1/200 of the total area of the tube was created at various locations along the length of the tubes. Four different locations of L_0 (L_0 = 0.5, 0.625, 0.75 and 0.875 L) were considered and the variation of elliptical holes with three different major axis lengths and aspect ratios were selected as the geometrical discontinuities to be investigated the influence of location in this section. The major axis of a cutout refers to the longer axis of the discontinuity which is perpendicular to the direction of compression. The corresponding force–deformation and mean force–deformation histories of the cylindrical thin-walled shell with a cutout under impact loading are shown in Figs. 7 and 8 and Table 1, respectively, with data from a control specimen without a cutout also shown. When cutout locations were located at 0.625 and 0.5 L, a greater crushing deformation caused by global bending and as the location of the cutout approached the load end (0.875 and 0.75 L), the deformation stops before it reaches a length of 120 mm. Due to the variance in deformation and to clarify the results by comparison, the numerical outcome considered herein end shortening of up to 120 mm of the thin-walled cylinder tube.

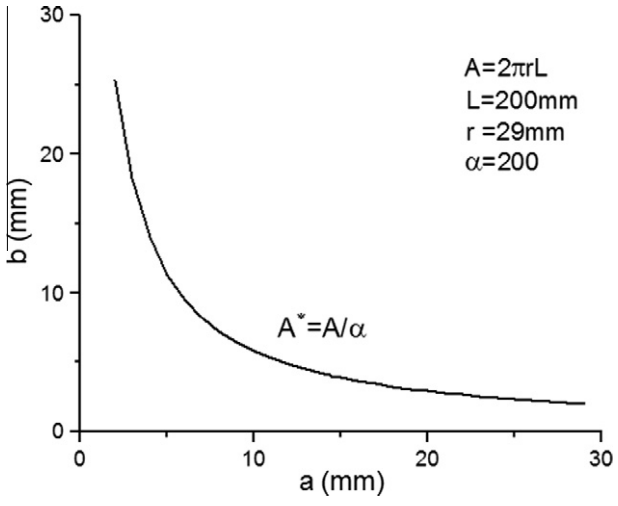

Fig. 5. Relation between radii a and b for an elliptic cutout on cylindrical shell.

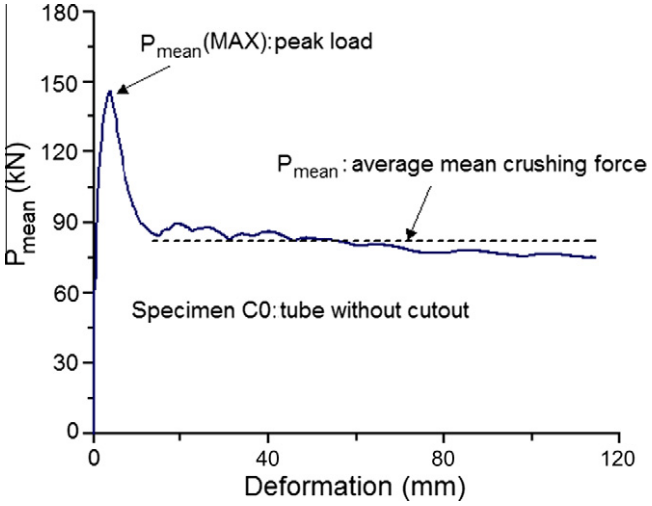

Fig. 6. The description of axial mean crushing force.

These results show that the cutout location along the shell's height had a significant influence on energy absorbing capacity. For all types of cutout, the results showed slight variations in the first peak force as the cutout location changed from 0.5 to 0.875 L. After reaching the first peak crush load, the rapid decrease in crushing force results from the formation of plastic hinge. However, the overall results of collapse mode were very different. Results for cutouts located near the loaded end (0.875 and 0.75 L) approached of the tube without cutout than the others. The collapse behavior was very similar so that the energy absorbing ability was similar. It reveals that though the two locations of cutout lead to local buckling around the cutout, but it did not cause globing bending. Furthermore, after the plastic buckle initiated from the cutout, the buckle remained stable and underwent progressive irregular folding, which could be due to uneven distribution of impact force on the geometric discontinuities. However, when the cutout was located at its mid-height, a transition from progressive buckling situation to a global bending mode would take place and the energy absorbing ability will be severely reduced. Considering the energy absorbing ability of the distal end shown in Fig 8, the P_{mean} of 120 mm for C10, C40 and C90 are 35.99, 40.94 and 34.97 kN, which decreased rapidly by 53.6%, 47.3%, and 55.0% in comparison with a tube without a cutout.

By and large, a comparison of energy absorption performances for cutout location of 0.625 L indicates that an elliptical discontinuity of aspect ratio 0.285 displayed a more stable deformation process. In brief, the stability of the crushing process and the accompanying energy absorption was observed to be higher for specimens with a shorter major axis length. We also observed that a variation in the type of the cutout can significantly influence its load bearing capacity.

In other words, shorter major axes form a long and narrow hole which is perpendicular to the direction of compression load, so that resistance to external forces is efficient. In contrast, when the cutout is composed of long major axis and short minor axis. The shape of geometric discontinuities was flat, which resistance is low. The cutout shape directly affects the load bearing capacity and further causes different collapse mode. Therefore, from the above analysis, it is clear that the influence of energy absorbing capacity and collapse folding depends strongly on the type and location of the cutout, expect cutout is at mid-height.

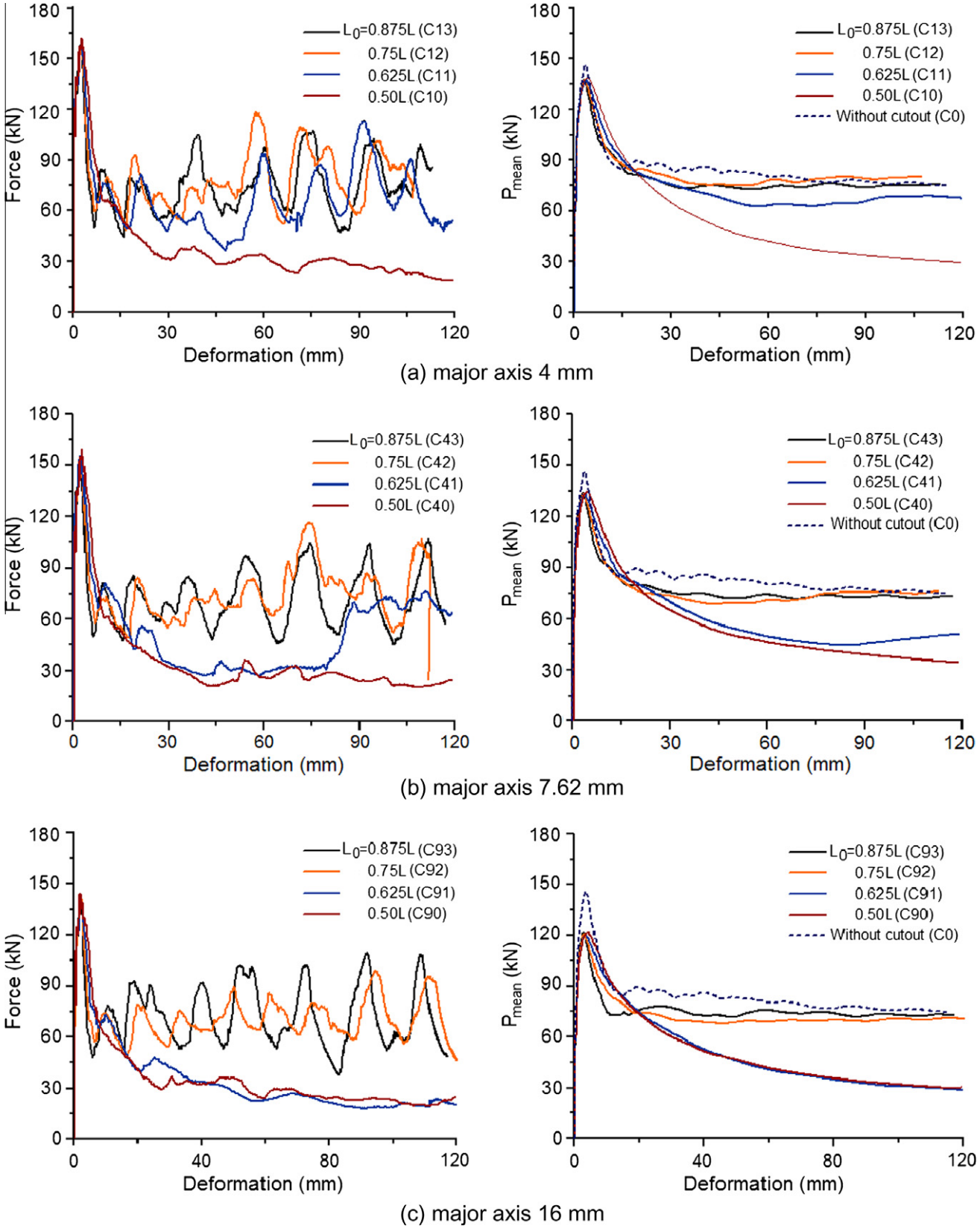

Fig. 7. Responses force–deformation history and mean force–deformation curves subject to dynamic impacting.

4.2. Influence of aspect ratio

Under progressive buckling, a cutout location at 0.75 L affected the collapse behavior more than a cutout location at 0.875 L. This section was mainly to investigate the effect on energy absorption capacity of different geometric discontinuities. The variations of elliptical holes of the same area with different major axis lengths were selected. Nine different major axis

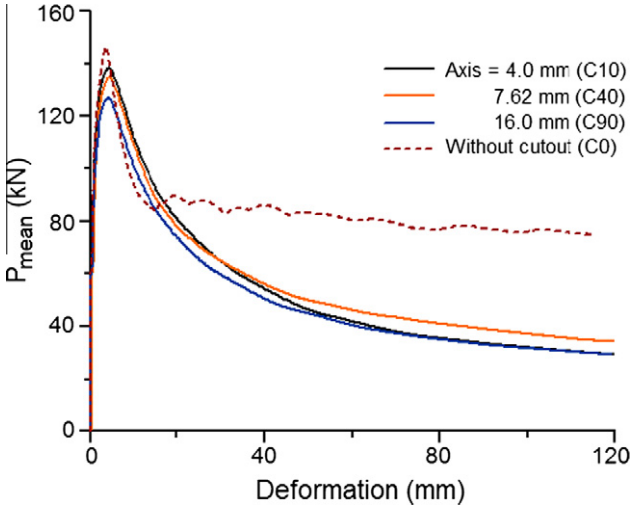

Fig. 8. Mean force–deformation for specimens of cutout located in 0.5 L and without discontinuity.

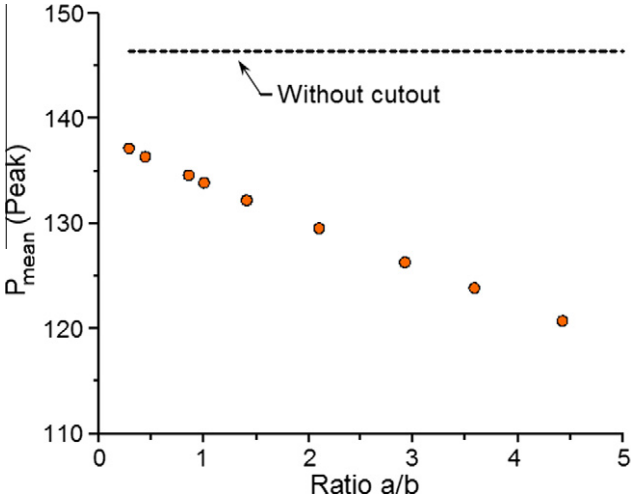

Fig. 10. Peak mean force against ratio of *a* to *b* from modeled results.

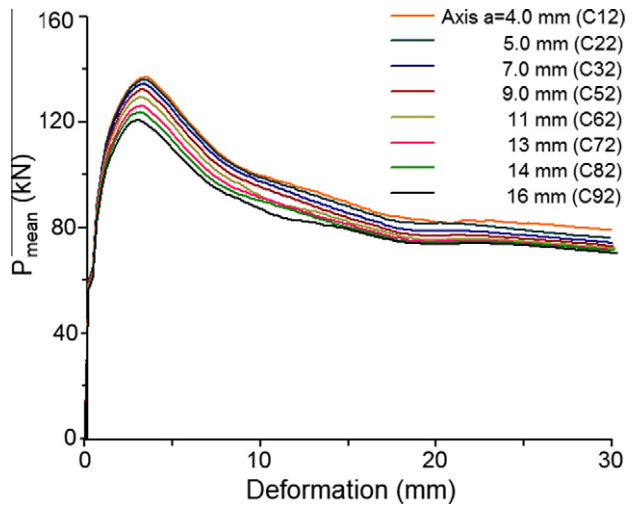

Fig. 9. The relationship between the mean axial crushing force and the deformation of 30 mm for different type cutout.

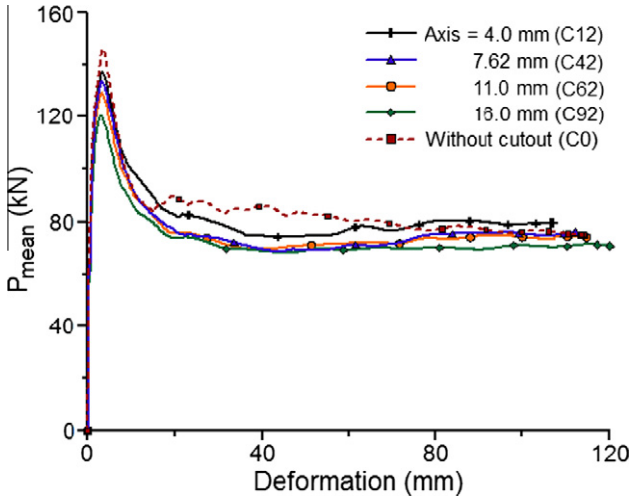

Fig. 11. Comparison in numerical simulation obtained mean force–deformation for C12, C42, C62, C92 and C0 (specimen without discontinuity).

lengths of the elliptical discontinuities were considered herein to examine the effect of the collapse mode and the energy absorbing efficiency.

Figs. 9–12 show results from a numerical study of the response of high strength steel cylindrical shells with various elliptic cutouts under dynamic impact. In order to observe the variations of the peak loading of different cutout clearly, Fig. 9 presents the relationship between the mean axial crushing force and the deformation of 30 mm. It can be seen from these curves that the peak value of P_{mean} increases, as the major axis length decreases for discontinuities. Fig. 10 shows the mean buckling value decreases almost gradually linearly as a function of the cutout's type.

Additionally, to clarify the results of the comparative, Fig. 11 plots the force–displacement curves under four major axis compared with a perfect tube. This shows that different types of cutouts not only influenced the peak load, but also caused the thin-walled component to produce more deformation. For instance, a cutout of major axis length of 4 mm leads to a 6.3% drop in the peak mean load and results in 8.55%, 11.50% and 17.52% decrease for the three types cutouts (C42, C62 and C92) than C0, respectively. The last crushing deformations of cutouts with major axis length of 7.62 and 11 mm are 112.41 and 115.77 mm, they were close to 114.51 mm of no cutout tube. But as the major axis lengths are 4 and 16 mm, the deformation was evidence different with others. Compare to C0, the last folding deformation of C12 was lower by about 6.4% and the displacement of C92 reached to 120.2 mm, which increased almost 4.97%. These results clearly show that these changes in peak loading and final deformation were strongly related to the geometric discontinuities, which led to different collapse mode.

Deformation patterns corresponding to selected points during the compression response are shown in Fig. 12; it reveals that the kind cutout of C12, the buckling mode was similar to the symmetric deformation mode resulting in efficient energy absorbing characteristics. In contrast, cutout of specimen C92 like a flat hole had a great effect on the irregular deformation and reduces the energy capacity. Otherwise, the peak force also differs from each other about 9.97%. This phenomenon becomes more significant as the major axis lengthens; it will cause a greater crushing deformation of the thin-walled tube and reduce the energy absorbing ability.

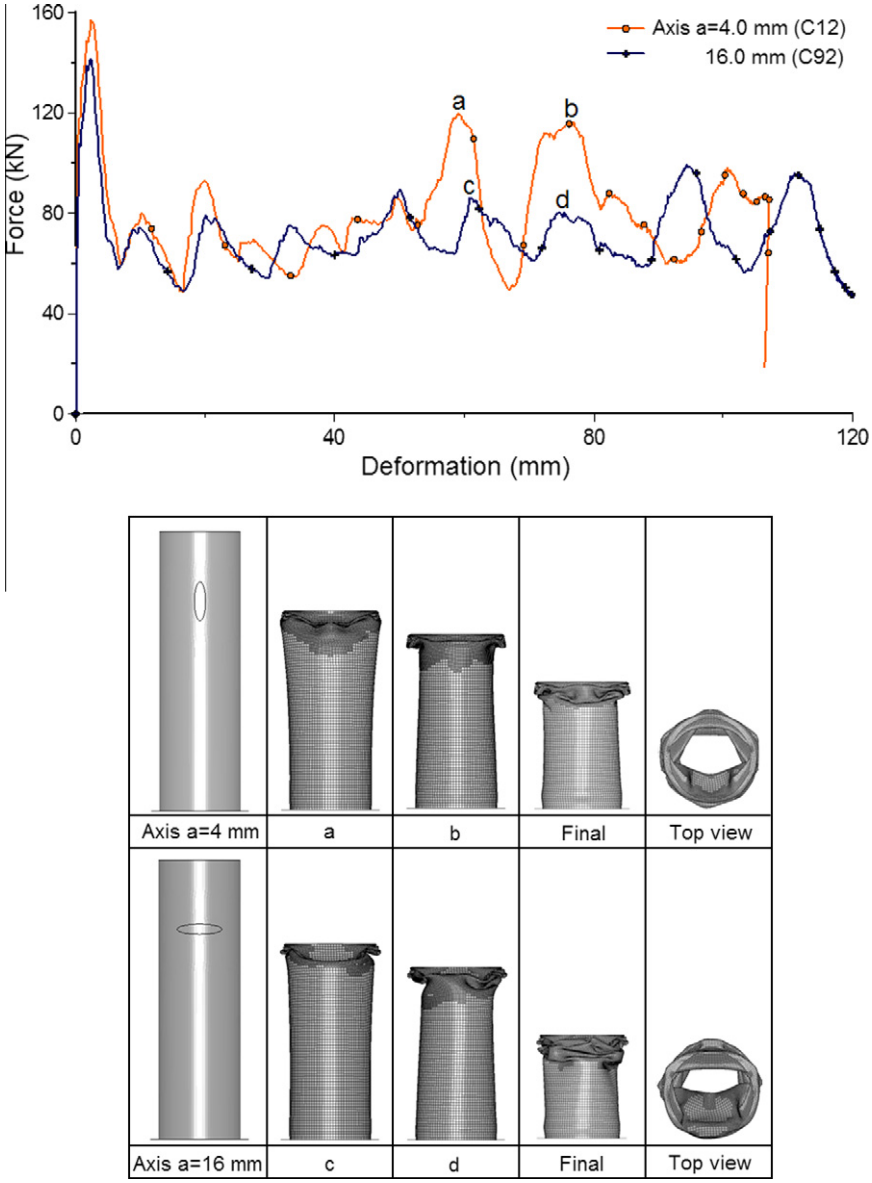

Fig. 12. Force–deformation curves and collapse profiles of the C12 and C92 the from simulations.

4.3. The effect of symmetry of geometrical discontinuities

Referred in Section 4.1, when the cutout is located near the mid-height of the tube, as a result of stress concentrations response near the cutout leads the collapse mode of the structures to global bending. This folding behavior rapidly decreased the energy absorbing capacity. It is interesting to investigate the symmetry of geometrical discontinuities as a deformation control method, it can be used to avoid failure resulting from global bending mode and change a mode that promoted greater energy absorption.

To understand the influence cutout symmetry on changing collapse mode of structures, three types of cutouts were selected to investigate the effectiveness of the symmetry of geometrical discontinuities and also compared with the results in Section 4.1. The results are shown in Figs. 13 and 14 and Table 1. Buckling behavior of compression-loaded cylindrical shells with geometrical discontinuities placed at opposite walls are shown in Fig. 13. The performance of global bending mode displayed highly similar force–deformation relationships of all specimens and the phenomenon were independent of the aspect ratios. However, the results also indicated that the use of symmetric cutouts changed certainly transition from global bending to progressive folding in the different collapse modes for three types of cutouts.

This was observed in specimen C94 with major axis length of 16 mm, which deformation in the regular progressive mode is more pronounced compared to unstable folding of C90. Furthermore, the variations of both types of collapse exhibited the largest peak crush load and peak mean crush loads level of the specimens were decreased rapidly with the large major axis length. For instance, Fig. 13(c) shows the differences of specimens C90 and C94, which had a peak mean crushing force 95.9 and 122 kN, respectively. This difference is primarily due to differences in the symmetry of the cutouts. Thus, it seems that the specimen which has a symmetrical cutout will be more efficient than the one which has single cutout when both specimens are subjected to the same set of test conditions. Similarly,

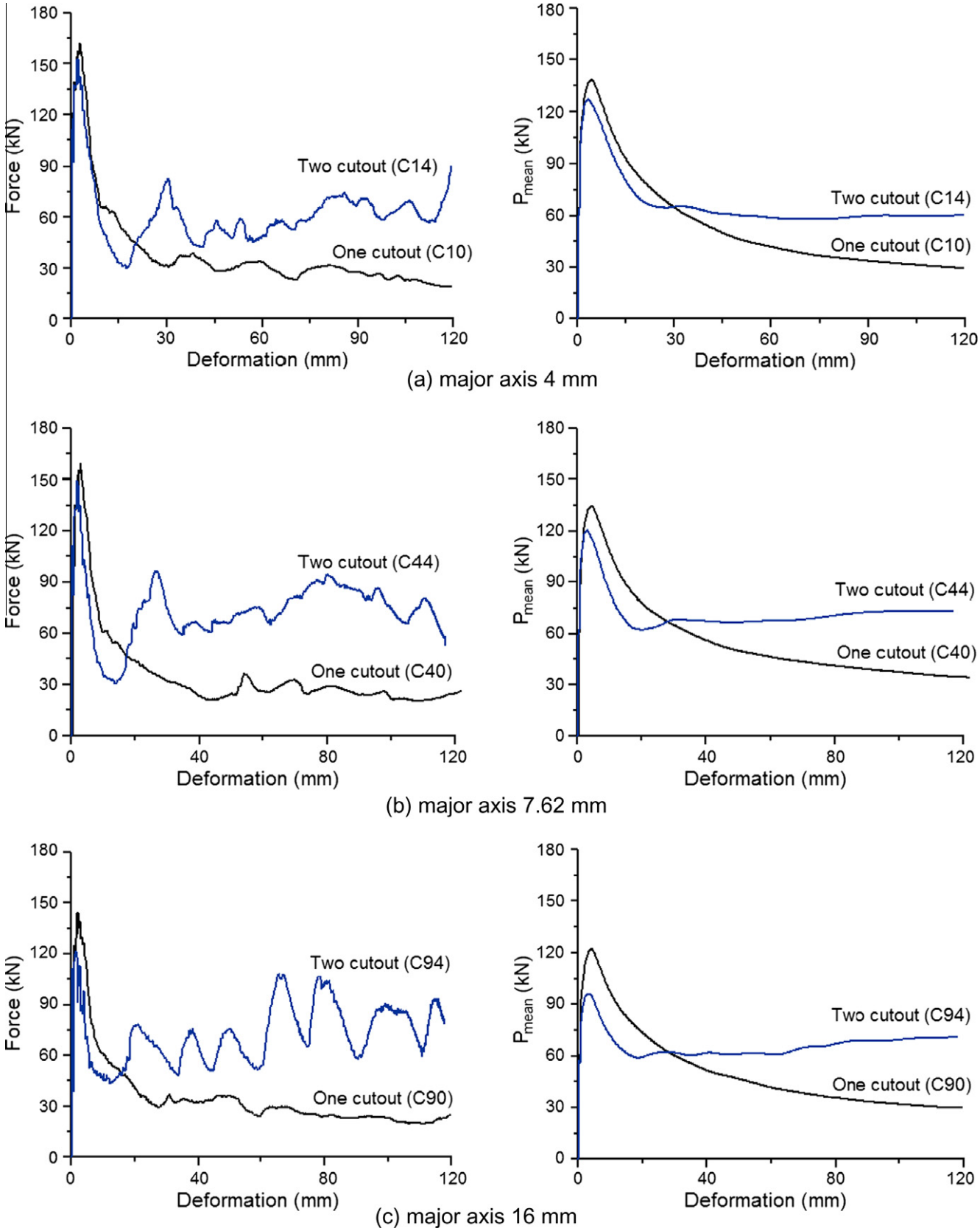

Fig. 13. Responses force–deformation history and mean force–deformation curves subject to dynamic impacting.

crush force efficiency, defined as the ratio of the mean crush load to the largest mean crush load. From Fig. 14, we can see simulations showed that as the major axis length increase, lead to the peak crush load decrease and appears most desirable

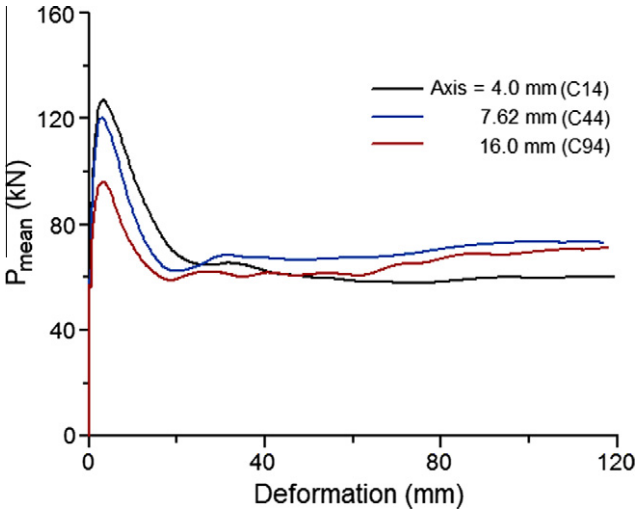

Fig. 14. Comparison of mean force versus deformation among three types of cutouts placed at opposite ends.

crush force efficiency. As an example, the value of C94 is 0.70, which has 31.43% and 15.71% larger crush force efficiency than the specimens of C14 and C44.

5. Conclusions

A systematic numerical investigation was carried out to examine the influence of high strength cylindrical tubes with elliptical discontinuities with varying major axis lengths and aspect ratios were completed. In addition, an investigation was also conducted to examine the crush performance of the symmetry and location of cutouts along the length of the shell. The numerical simulations provided valuable insight into the behavior of the shells, and enable us to understand the variations of tubes with cutouts.

Our results show that the location of cutout can significantly influence the buckling performances and energy absorbing capacity of the thin-walled tubes. The numerical results indicated that a cutout located at the mid-height of the cylindrical tube led to the collapse of global bending, whereas when the cutout was located near the loaded end, progressive buckling occurred. Specimens bucked in global bending mode displayed highly similar force–deformation relationships. Another important finding is that the longer the major axis length of the cutout, the more sensitive it is to changes in the cutout location.

The presence of a cutout with long axis length can significantly reduce the peak buckling force and cause a greater crushing deformation of thin-walled tubes. Additionally, as the major axis length of cutout rises, the mean buckling value decreases nearly linearly as a function of elliptical discontinuities. Results from numerical modeling of thin-walled tubes reveal that the buckling mode of cutout with short axis length was similar to the symmetric deformation mode leaded to energy absorbing efficiency becomes to well. In contrast, a cutout with long major axis length yielded an irregular folding collapse and decreased the energy absorbing capacity. Therefore, the length of major axis effects dominated during collapse deformation mode of the specimens.

It is worth noting that a transition from global bending modes to progressive folding modes could occur when the two cutouts were located at opposite walls. Specimen C94, which contained an elliptic hole with a major axis length of 16 mm, had the highest crush force efficiency of 0.70. Due to the result of analysis, specific cases are presented that suggest that two cutout located symmetrical in a shell can be tailored to achieve improved buckling response characteristics. Therefore, if shell structures contain cutouts are designed to achieve specific desired results, the symmetry of discontinuities is an important factor to consider.

References

[1] J.M. Alexander, An approximate analysis of the collapse of thin cylindrical shells under axial loading, Q. J. Mech. Appl. Math. 13 (1960) 10–15.
[2] W. Abramowicz, N. Jones, Dynamic axial crushing of square tubes, Int. J. Impact Eng. 2 (2) (1984) 179–208.
[3] M. Yamashita, M. Gotoh, Y. Sawairi, A numerical simulation of axial crushing of tubular strengthening structures with various hat-shaped cross-sections of various materials, Key Eng. Mater. 233 (2002) 193–198.
[4] N. Jones, Structural Impact, Cambridge University Press, Cambridge, 1989.
[5] W. Abramowicz, N. Jones, Dynamic progressive buckling of circular and square tubes, Int. J. Impact Eng. 4 (4) (1986) 243–270.
[6] M. Langseth, O.S. Hopperstad, Static and dynamic axial crushing of square thin-walled aluminum extrusions, Int. J. Impact Eng. 18 (1996) 949–968.
[7] D.A.I. Galib, A. Limam, Experimental and numerical investigation of static and dynamic axial crushing of circular aluminum tubes, Thin-Walled Struct. 42 (2004) 1103–1137.
[8] K.R.F. Andrews, G.L. England, E. Ghani, Classification of the axial collapse of cylindrical tubes under quasi-static loading, Int. J. Mech. Sci. 25 (1983) 687–696.
[9] Qingwu Cheng, William Altenhof, Li Li, Experimental investigations on the crush behavior of AA6061-T6 aluminum square tubes with different types of through-hole discontinuities, Thin-Walled Struct. 44 (2006) 441–454.
[10] Haipeng Han, Farid Taheri, Neil Pegg, Quasi-static and dynamic crushing behaviors of aluminum and steel tubes with a cutout, Thin-Walled Struct. (2007).
[11] Haipeng Han, Jinquan Cheng, Farid Taheri, Neil Pegg, Numerical and experimental investigations of the response of aluminum cylinders with a cutout subject to axial compression, Thin-Walled Struct. 44 (2006) 254–270.
[12] Hsuan-The Hu, Su Su Wang, Optimization for buckling resistance of fiber-composite laminate shells with and without cutouts, Compos. Struct. 22 (1992) 3–13.
[13] LS-DYNA Theoretical Manual, V.971, Livermore Software Technology Corporation, Livermore, CA, USA, 2006.
[14] J. Mark, F.G. Holst, J. Michael Rotter, Axially compressed cylindrical shells with local settlement, Thin-Walled Struct. 43 (2005) 811–825.
[15] W. Abramowicz, N. Jone, Dynamic progressive bucking of circular and square tubes, Int. J. Impact Eng. 4 (1986) 243–270.